Paper D

CO_2 storage in the Utsira Formation – ATHENA 3D reactive transport simulations

Hellevang, H.
Khattri, S.K.
Fladmark, G.E.
Kvamme, B.

Submitted to *Basin Research*

CO_2 storage in the Utsira Formation – ATHENA 3D reactive transport simulations

H. Hellevang[*], S. K. Khattri[†], G. E. Fladmark[†], B. Kvamme[*]

[*]*Department of Physics and Technology, University of Bergen, Allégt. 55, 5009 Bergen, Norway*
[†]*Department of Mathematics, University of Bergen, Johannes Brunsgate 12, 5008 Bergen, Norway*

ABSTRACT

Emissions of CO_2 to the atmosphere by combustion of hydrocarbons and by CO_2 capture from natural gas streams are believed to contribute to a global greenhouse effect. It has for this reason been suggested to inject captured CO_2 back into geological formations where major point sources of CO_2 are available. Statoil has since 1996 injected captured CO_2 from the Sleipner West facility into the Utsira Formation (Korbøl & Kaddour, 1995). The injection has been periodically monitored by seismic surveys through the injection area. The seismic monitoring provides indications of how the immiscible part of the injected CO_2 is moving. It provides however no information about the reactivity of injected CO_2 with the reservoir minerals.

ATHENA is a thermal multiphase 3D-reactive-transport numerical code that has been developed to simulate long-term large-scale reactive flow of CO_2 in porous media. The code is separated into the ATHENA multiphase flow code, and the newly developed ACCRETE reaction module. The ATHENA code is used in this study to simulate 20 years of 1Mt annual injection of CO_2 and 980 years of post-injection natural migration in the Utsira Sand. A system that comprises the central 2.25 km^3 of the Utsira Sand around the injection point has been simulated. The system consists of sandy units separated by discontinuous clayey horizons.

Simulations show that injected CO_2 rise buoyantly mainly through discontinuities in clayey horizons and accumulate beneath topographic highs in the top-Utsira surface. As the CO_2 is injected pH drops to approximately 4.9 at full saturation in equilibrium with calcite. Most of the system approaches this pH after a few hundred years. The acidic condition induces dissolution of primary phyllosilicates and precipitation of carbonates. The dominant carbonates that form are magnesite and siderite, whereas dawsonite ($NaAl(OH)_2CO_3$) only forms a minor precipitate at high CO_2 saturations. Simulations that include a regional flow through the system shows that CO_2-water-rock interactions are locally dependent on hydrodynamic conditions.

INTRODUCTION

Increasing atmospheric concentrations of greenhouse gases emitted from anthropogenic sources may potentially lead to global climate changes. Because carbon dioxide is considered as a major greenhouse gas, different strategies have been suggested of how to reduce emissions. Storage of CO_2 in geological formations, e.g. coal seams, depleted oil reservoirs, producing oil reservoirs, or saline aquifers, are options that are currently being investigated (e.g., Lohuis, 1993; Bachu et al., 1994; Gunter et al., 1996; Saylor et al., 2001; Baines & Worden, 2004; Bouchard & Delaytermoz, 2004).

Several CO_2 storage projects are at present active or planned to start in the near future.

Correspondence: H. Hellevang, Department of Physics and Technology, University of Bergen, Allégt. 55, 5009 Bergen, Norway. E-mail: helgeh@ift.uib.no

The first industrial scale site which is still operative is the Sleipner injection site in the North Sea which injects captured CO_2 into the Utsira formation (Korbøl & Kaddour, 1995; Zweigel *et al.,* 2001; Torp & Gale, 2004). Sites like Snøhvit (Northern Norway; Maldal & Tappel, 2004) and In Salah (Algerie; Riddiford *et al.,* 2004) are shortly to follow. The annual combined reduction from the Sleipner and Snøhvit injection sites are estimated to 1.7 million tonnes. Once CO_2 is injected it starts to dissolve into the formation water and any excess gas or fluid CO_2 will migrate buoyantly towards the top of the formation and accumulate beneath low-permeable structures. This excess CO_2 migration is of major importance on the short-term safety of the injection site. The dissolved CO_2 reacts with the water to form carbonic acid and lower the pH. This in turn makes the water reactive with respect to the minerals present in the reservoir. Dissolution of these minerals leads to formation of new minerals such as solid carbonates.

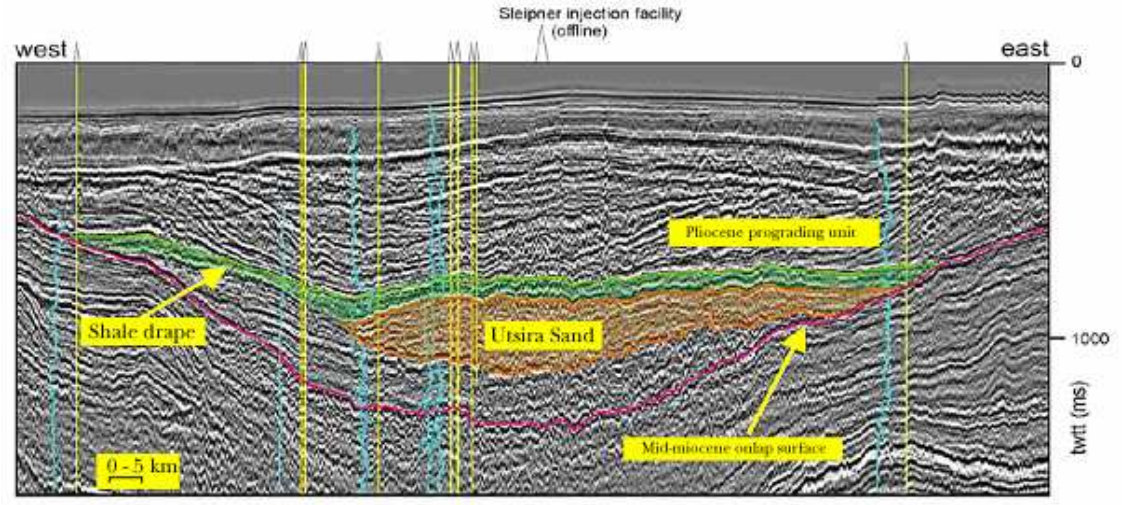

Fig. 1. East-west Seismic profile through the injection zone. Modified from Torp and Gale, (2004).

Once formed these carbonates may contribute to a safe long-term storage of CO_2.

Since mineral reactions are slow at temperatures normally encountered in storage settings (some silicate grains may need thousands of years before disintegrating, Lasaga, 1998), the direct value of experimental work on CO_2-water-rock interactions is limited and can only provide a glimpse into the qualitative and quantitative nature of the reactions. To access information on the long-term fate of the CO_2, i.e. reactions lasting for hundred to thousands of years, numerical codes that integrate results from various geochemical experiments have to be used.

The aim of this work is to present new 3D reactive transport simulations of the Utsira injection site using the ATHENA thermal multiphase-flow research code coupled with the ACCRETE geochemistry module. The simulations illustrate how 1000 years of interactions between CO_2, formation water and the solid mineral framework affects the chemistry of the system, illustrated by pH, and how the interactions result in permanent storage of CO_2 in solid carbonates. The effect of a regional flow of formation water on CO_2-water-rock interactions is also examined.

MODELLING OF THE UTSIRA FORMATION

Utsira Formation geology

The Utsira Formation comprises basinally restricted sediments mainly deposited from Middle- to Late Miocene up to Early Pliocene into the northern North Sea. The formation consists mainly of fine sands and silts interrupted by thin clay horizons. The sandy part of the formation, termed as the Utsira Sand, corresponds to the sandy part of the Utsira Formation. The sands extend for more than 400 km from north to south, reaching up to approximately 100 km in an east-west direction, and cover a total area of more than 26.000 km^2 (e.g., Torp and Gale, 2004; Chadwick *et al*., 2004). The deposition of the sands is divided into two depositional centres laying in the southern and northern part respectively. The two depositional centres are separated by a shallower and thinning saddle-like part (Fig. 1). The thickness of the sand is largest in the depositional centres with the maximum depth of more than 300 meters reached in the southern depocenter (Chadwick *et al*., 2004).

The Utsira Formation has been defined regionally based on approximately 16.000 line km of 2D seismic data and information from 132 wells that penetrates the reservoir unit (Chadwick *et al*., 2004). In addition to this regional mapping more detailed mapping using 3D seismic techniques have been used around the CO_2 injection zone at Sleipner.

The lower boundary of the Utsira Formation is regionally recognized as a strong seismic reflection that separates the slightly transparent sandy reflections from deformed and faulted reflections below, whereas the upper seismic boundary of the Utsira Formation is recognized below a regional seismic downlap surface (Gregersen *et al*., 1997). Two seismic units of almost equal thickness can be distinguished regionally. The lower seismic unit is interpreted to consist mainly of sand with minor intercalations of clay and shows semicontinuous bidirectional downlapping, whereas the upper unit that is interpreted to consist of interbedded clays with minor sands shows slightly prograding downlapping reflections (Gregersen *et al*., 1997; 2000). The CO_2 is injected in the lower sandy unit. Fig. 1 shows an east-west profile through the CO_2 injection area. The profile covers reflectors from the pre-Miocene basement of the Utsira Sand up to the most recent sediments.

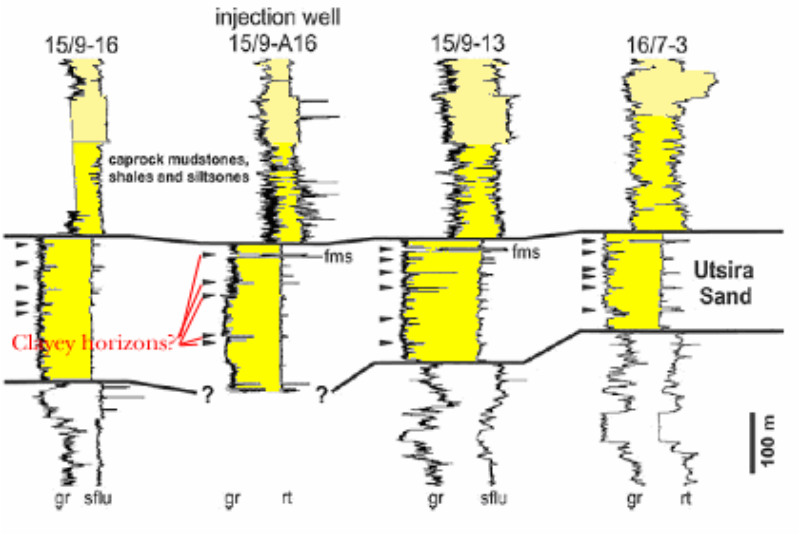

Fig. 2. Resistivity logs (rt) and gamma-ray logs (gr) indicate the sandy Utsira Sand and several peaks that suggest clayey horizons. Modified from Chadwick *et al*., (2004).

Central in the figure is the Utsira Sand that pinches out in the east-west direction towards the underlying Lower Nordland Shales. Fig. 1 also shows the thick sequence of prograding units that mainly consist of clay with minor sands that is separated from the Utsira Sand by strong seismic reflections.

Gamma-ray- and resistivity logs show Utsira Formation as blocky patterns that is clearly separated from units above and below by a sharp drop in values (Gregersen *et al*., 1997). Internally the lower gamma-ray values of the sands are typically separated by several short intervals with higher values that are interpreted to represent clayey intervals. Fig. 2 shows gamma-ray- and resistivity logs at an east-west traverse through the Sleipner injection area. The drop in values from both underlying and overlying units is clear. Also illustrated are several more or less pronounced peaks of higher values. These peaks have been interpreted to be thin clayey horizons that separate the Utsira Sand into several sandy subunits (Chadwick *et al*., 2004). Comparisons between seismic images before and after CO_2 injection started in 1996 support this interpretation (e.g., Zweigel *et al*., 2001).

Petrographic studies of core samples and cuttings suggest that the Utsira Sand mainly consists of uncemented fine-grained sand dominated by quartz with minor feldspars and carbonates in shell fragments (Chadwick *et al*., 2004). The porosity of the sand is in most of the reservoir in the range 35-40%. The Plioence clay horizons that constitutes the caprock of the Utsira Sand consists mainly of clayey silts or silty clays with minor coarser sediments. Samples from wells that are close to the Utsira injection site shows that the clays mainly consists of kaolinite, micas and quartz, with minor feldspars and carbonates (Chadwick *et al*., 2004). Table 1 provides more details on the mineralogy of the Utsira Sand and clays.

Table 1.
Generalized mineralogy and porosity from Utsira Sand based on whole-rock XRD analysis and Utsira Caprock based on analysis of cuttings. From Chadwick *et al*., 2004.

	Mineral %	
Minerals	**Utsira Sand**	**Utsira Caprock**
Quartz	75	30
Calcite	3	3
K-feldspar	13	5
Albite	3	2
Aragonite	3	0
Micas	3*	30
Kaolinite	0	14
Smectite	0	3
Chlorite	0	1
Pyrite	0	1
Gypsum	0	1
Halite	0	2
Sylvite	0	1
Barite	0	5
porosity	35-40%	

*Referred to in Chadwick *et al*. (2004) as Micas and others.

Numerical model

To gain information about interactions between CO_2, formation water, and formation minerals in the Utsira Formation, the 3D thermal multiphase-flow research code ATHENA has been used. The code is separated

into the ATHENA flow code, and the newly developed ACCRETE geochemistry module (Hellevang & Kvamme, 2006).

The ATHENA simulator

The ATHENA simulator is based on the SOM (Secondary Oil Migration) model which was originally developed for hydrocarbon migration in sedimentary basins and was first presented in 1997 (Fladmark, 1997; Elewaut, 1997). This 3-dimensional secondary oil migration simulator has since then been continuously expanded and improved to cover a wide range of features and geological scenarios (e.g., Reme & Øye, 1999; Reme *et al*., 2000; 2002; Øye, 1999; Øye & Reme, 1999; Qin *et al*., 2000; Garrido *et al*., 2004). The latest branch of the code that is currently under development is a model capable of simulating large-scale multiphase reactive transport of CO_2 storage scenarios. This has among other things lead to inclusion of new meshing routines for complex reservoir geometries and the development of the ACCRETE geochemistry module (Hellevang & Kvamme, 2006).

During CO_2 storage simulations, ATHENA separates the system into a water phase, a gas phase, and a solid matrix. The water phase consists in the present study of 14 components with concentrations that are updated by the ACCRETE geochemistry module. The chemical components follow the water phase during water movement. Molar quantities like molar masses and molar fractions of components in the water phase, as well as saturations, volumes and densities of phases are estimated by flash calculations. The geologic formation is divided into static finite volumes each with a volume V and surface boundary S and unique macroscopic properties like porosity and permeability. All phases can be present simultaneously in one finite volume. By denoting m_p as the mass of component p, a mass balance equation for component p in a finite volume can be expressed by:

$$\frac{\partial}{\partial t}\int_V m_p + \int_V \nabla \cdot \mathbf{m_p} = \int_V q_p \,, \qquad (1)$$

where the subscript V on an integral sign indicates that it is a volume integral, $\mathbf{m_p}$ denotes the mass flux density of component p, and q_p is the source term. It follows from this equation that the rate of change of p in the control volume is equal to the rate which p is being generated in the reaction term, minus the flux of p through bounding surfaces. The total amount of the component in the finite volume is calculated according to:

$$N_p = \int_V m_p \,. \qquad (2)$$

Since water pressure is one of the primary variables an equation based on the volume balance method is constructed as:

$$R = V_p - \sum_{l=w,g} V^l \,, \qquad (3)$$

where R is the difference between the pore volume V_p, and the total volume of the gas and water phases. This difference R is a function of the water pressure P^w, the overburden pressure W, and the molar mass of each component and has to be zero at all time. Linearizing R by the Taylor Series expansion in time and by putting the resulting $R(t + \Delta t)$ equal to zero and use the chain rule for $(\partial R / \partial t)$ results in the equation for water pressure:

$$\frac{\partial R}{\partial P^w}\frac{\partial P^w}{\partial t} + \sum_{i=1}^{n_c}\frac{\partial R}{\partial N_i}\frac{\partial N_i}{\partial t} = -\frac{R}{\Delta t} - \frac{\partial R}{\partial W}\frac{\partial W}{\partial t} \qquad ,(4)$$

The CO_2 gas phase pressure is provided in terms of the water phase pressure and the capillary pressure between the water and CO_2 phase according to:

$$P^{CO_2} = P^w + P_c \,. \qquad (5)$$

The Darcy velocity $\mathbf{v}$ for phase l is calculated according to:

$$\mathbf{v}^l = -K\frac{\kappa^l}{\mu^l}\left(\nabla P^l - \gamma^l \nabla d\right), \qquad (6)$$

where K and κ denote absolute and relative permeability respectively, μ is viscosity, γ is the product of gravity and density of phase l, and d is depth. For deriving the temperature T for a control volume the following energy conservation equation is used:

$$\frac{\partial}{\partial t}\int_V \rho u - \int_S k\nabla T = -\int_S h\rho\mathbf{u} + \int_V q \,, \qquad (7)$$

where ρu represents the heat capacity term, $h\rho\boldsymbol{u}$ the convective flux, $k\nabla T$ the conductive flux and q the heat source density.

The ACCRETE geochemistry module

ACCRETE is an acronym for **A**thena **C**arbon **C**apture and sto**R**age geoch**E**mis**T**ry modul**E**. The development of the code was initiated as the Athena code was expanded to cover geologic storage of CO_2. The ACCRETE module is called as an external object from the Athena code for each control volume and for each timestep. Reactions included are those generally believed to play a significant role during CO_2 storage. Interactions between a total of 16 mineral phases, 13

aqueous solutes, H_2O solvent, and CO_2 as a separate gaseous or supercritical phase are at present being calculated (ACCRETE v.1.0).

Thermodynamic data for mineral reactions and aqueous speciation is calculated by the SUPCRT92 program (Johnson *et al*., 1992) using the dprons96.dat database. The standard state adopted in this study is that of unit activity for pure minerals and H_2O at any temperature and pressure. For aqueous species other than H_2O, the standard state is unit activity of the species in a hypothetical 1 molal solution referenced to infinite dilution at any temperature and pressure. For gases, the standard state is for unit fugacity of a hypothetical ideal gas at 1 bar pressure.

Equilibrium constants for reactions are calculated from standard state free energies of formation of the constituent components. The temperature dependence of the equilibrium constants is given by a Van't Hoff type of expression neglecting any temperature dependence on the enthalpy. This provides sufficient accuracy since the volumetric effects on the enthalpy is small in the liquid phase. The difference in specific heat capacities across the reaction is more reaction individual but in many cases the effect is negligible relative to other sources of errors.

The demands for a satisfactorily solved geochemical system is that the solution is mass balanced and charge neutral, and that equilibrium considerations (e.g. the carbonate system) are solved. The charge neutrality is achieved by defining the activity of the H^+ ion as the sum of charges of all N other charged species in the water phase. Activity for all charged species is calculated according to the Truesdell-Jones equation (Truesdell & Jones, 1974) that is valid for up to 2*N NaCl* dominated solutions. Ion-specific parameters for the Truesdell-Jones activity model are listed in Table 2. The aqueous speciation is strongly a function of the amount of CO_2 that is allowed to dissolve into the water phase. The bubble point mole fraction of CO_2 is estimated as a function fugacity calculated using the SRK EOS as a function of temperature and pressure, and Henrys Law coefficient as a function of temperature and salinity according to:

$$x_{CO_2}^b = \frac{P\phi}{K_H} \cdot \exp\left\{\frac{\bar{v}^\infty}{RT}(1-P)\right\}, \qquad (8)$$

Hellevang & Kvamme (2006) evaluated expression (8) and demonstrated that this equation provides a good estimate of the solubility of CO_2 in saline solutions at various temperatures and pressures. After activity coefficients and total dissolved carbon are calculated, speciation of the dissolved carbon is solved by an iterative procedure.

The next step after computing the initial solution is to solve the mineral reactions. The magnitude of the reactions, except for calcite that is assumed in instant equilibrium with the solution, is constrained by the kinetics given by:

$$r_i = k_i S_i \left(10^{\frac{\Delta G_T^{eq} - \Delta G_T(\mathbf{X})}{2.303RT}} - 1 \right), \qquad (9)$$

where k and S are kinetic constant (mol/m^{2}s) at temperature T and reactive surface for the reactions respectively, and $\Delta G_T^{eq} - \Delta G_T(\mathbf{X})$ is the difference between free energy at temperature T of the mineral reaction at equilibrium and at the actual water chemistry. The reaction rate is thus strongly a function of the aqueous component vector $\mathbf{X}$. The reactive surface area for dissolution is regarded to be proportional to the mass of the phase present, and for precipitation assumed equivalent to a fraction of the total surface area present in the reservoir (0.01 in this study). The kinetic constants at temperature T is calculated according to:

$$k = k_\theta \cdot \exp\left\{-\frac{E_a}{R}\left(\frac{1}{T} - \frac{1}{T_\theta}\right)\right\}, \qquad (10)$$

where E_a is the apparent activation energy for the reaction and R is the gas constant and subscript θ denotes the standard state temperature of 298.15 K. The change for aqueous component i that accompany the mineral reactions can be expressed as:

$$\mathbf{X} = \Delta t \cdot \mathbf{rv}, \qquad (11)$$

where $\mathbf{r}$ is an 1×16 matrix that contains all rates calculated according to expression (9), $\mathbf{v}$ is a 16×15 matrix that contains the stoichiometric number of aqueous components in the reactions, and Δt is the size of the timestep. The latter value is reduced in size if the mineral reactions result in negative concentrations for any of the aqueous components. Once an appropriate timestep is found, the resulting aqueous solution is recalculated to satisfy carbon- and charge balance. The mineral reactions are solved once the total time for all subtimesteps equals the predefined global timestep as directed by the ATHENA. Calcite is solved as an equilibrium reaction rather than constrained by kinetics since the calcite reaction is assumed to be several order of magnitude faster than the other reactions and is usually expected to reach a close to equilibrium state after only a few hours or days. This assumption is justified by experimental work on reservoir sand at reservoir conditions (e.g., Czernichowski-Lauriol et al., 2002).

The GMV graphical tool

The Graphical Mesh Viewer (GMV), developed at the Los Alamos National Laboratory is used to illustrate the meshing of the Utsira Sand at the Sleipner injection site, and the temporal and spatial evolution of CO_2, chemicals and minerals in this study (Fig. 3 to 13).

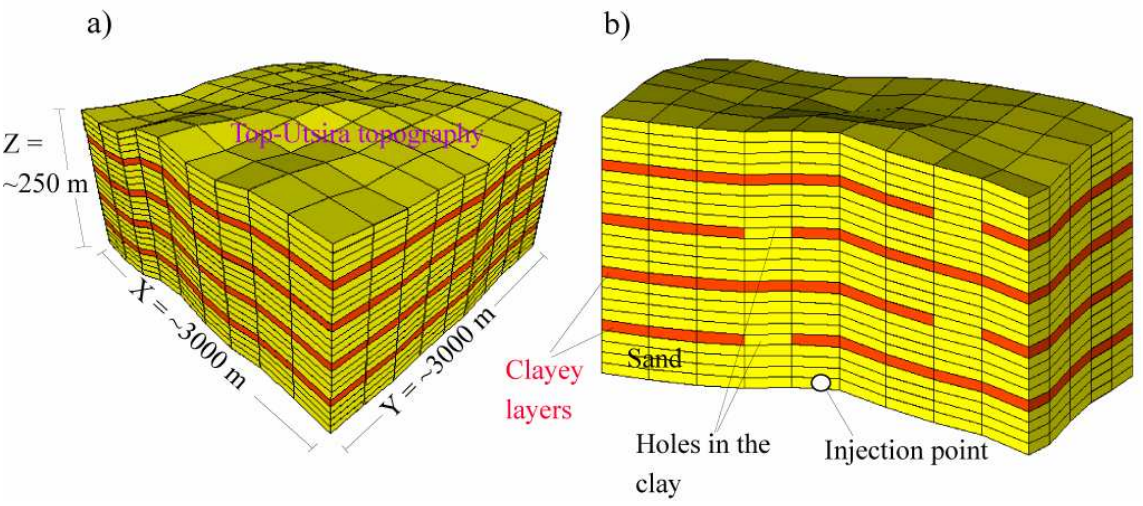

Fig. 3. Meshed Utsira formation at the Sleipner injection site a) Shows the size of the system, the spatial directions and the topography. The total volume of the meshed area is approximately 2.25 km^3. b) shows a cutplane section (XZ) through the central part of the system where the injection point and holes in the clayey layers occur.

Plotting isovolumes and cutplanes proved very valuable in presenting our 3D simulations. See the GMV manual at *http://www-xdiv.lanl.gov/XCM/gmv/doc.color.pdf* for more detailes on the software.

Simulation setup

The simulation setup is based on the Utsira Sand at the Sleipner injection site. The depth of the injection is at approximately 1000 meters below sea level which gives an approximate temperature and hydrostatic pressure of about 310 K and 100 bar respectively. We have simulated a volume of 3000x3000x250 m^3 meshed into 9x9x24 grids with CO_2 injected in the central lowermost grid (Fig. 3). The injection rate for the first 20 years of the simulations is approximately 1 Mt annual injection which corresponds to the injection rate of the Sleipner injection site (Korbøl & Kaddour, 1995). The injection is stopped after 20 years, which also corresponds to the final target of the Sleipner injection (Chadwick *et al*., 2004). Post-injection interactions between CO_2, formation waters and minerals are followed for another 980 years.

The higher spatial resolution in the Z direction of the meshed formation is to include clayey layers as suggested by both well logs penetrating the Utsira Formation (Gregersen *et al*., 1997), and seismic profiles that are shot after injection started in 1996 and compared to the 1994 seismic profile (Chadwick *et al*., 2004). We have included five sand units separated by discontinuous low-permeable clayey layers (Fig. 3). The discontinuity of the clayey layers is suggested by rapid upward migration of CO_2 through the clayey layers (Chadwick et al., 2004),. The discontinuities are added by inserting grids with sand properties in-between the clay. This is done in the central XZ plane shown in the cutplane in Fig. 3b.

The topography of the top-formation and intra-reservoir horizons are meshed based on seismic data provided by Statoil. For simplicity we use the same topography for all XY-surfaces from base to top in the formation (Fig. 3).

We separated simulations into two main scenarios, with and without regional formation water flow affecting the CO_2-water-rock interactions. In the simulation that includes a regional flow we induce a formation water flux through the YZ boarders of the mesh along the XZ plane from left to right in the cutplane of Fig. 3b. In both types of simulation scenarios an outlet on the right hand side is open to ensure hydrostatic pressure.

The primary and possible secondary minerals used in the simulations are listed together with kinetic data in Table 3. Primary minerals are adapted from the Utsira Sand mineralogy as reported by Chadwick *et al*., (2004) and listed in Table 1. Minerals that are missing in the ACCRETE thermodynamic database are replaced by similar minerals (similar by mineral group and/or similar by cation content). Also listed are a number of possible secondary minerals including carbonates like magnesite, siderite, and dawsonite, as well as possible secondary hydroxides and silicates. Kinetic data for the mineral reactions are, with some exceptions, adopted from a compilation in Johnson *et al*. (2001; 2004). The exceptions are dawsonite (Hellevang *et al*., 2005), gibbsite (Ganor *et al*., 2005), and labradorite (Carroll & Knauss, 2005), whereas annite, used as a proxy for glauconite, is assumed to have same kinetic properties as phlogopite (Table 3).

Table 3.
Initial volume fractions of minerals in sand and clay respectively and kinetic parameters for expressions (9) and (10).

Mineral	x^{Sand}	x^{Clay}	k_{25} (mol/m^{2}s)	Ea (kJ/mol)	S (cm^2/cm^3)
Calcite	0.039[1]	0.03	Equilibrium	62.8	$1.00x10^{2}$
Magnesite	0	0	$1.00x10^{-9}$	62.8	$1.00x10^{2}$
Siderite	0	0	$1.00x10^{-9}$	62.8	$1.00x10^{2}$
Dawsonite	0	0	$3.06x10^{-11}$	62.8	$2.44x10^{4}$
Albite	0.020	0.03	$1.00x10^{-12}$	80.3	$8.75x10^{2}$
Microcline	0.085	0.06	$1.78x10^{-13}$	51.7	$1.11x10^{3}$
Quartz	0.488	0.30	$1.04x10^{-14}$	87.7	$5.74x10^{2}$
Chalcedony	0	0	$3.45x10^{-13}$	87.7	$1.25x10^{4}$
Kaolinite	0	0.14	$4.00x10^{-13}$	29.0	$1.25x10^{4}$
Clinochlore-14A	0.003	0.03	$3.00x10^{-13}$	88.0	$1.25x10^{4}$
Daphnite-14A	0.003	0	$3.00x10^{-13}$	88.0	1.25x104
Muscovite	0.006	0.11	$1.00x10^{-13}$	22.0	$1.25x10^{4}$
Phlogopite	0	0.11	$4.00x10^{-13}$	29.0	$1.25x10^{4}$
Annite	0.006[2]	0.09[2]	$4.00x10^{-13}$	29.0	$1.25x10^{4}$
Labradorite	0	0	$2.04x10^{-10}$	42.1	$8.06x10^{2}$
Gibbsite	0	0	$3.16x10^{-12}$	53.0	$8.66x10^{3}$
Porosity	0.350	0.100			

[1]Calcite represents both the calcite and aragonite reported in the Utsira Sand
[2]Annite is used as a proxy for glauconite in the absence of thermodynamic and kinetic data

Table 4 lists the initial formation water chemistry. The data is adapted from Johnson *et al*. (2001; 2004) that in turn adapted data from a water sample collected at Oseberg some 200 km north of the Sleipner injection facility. This water chemistry is assumed to be representative for porewater in the Utsira Reservoir.

Table 4. Initial water chemistry for the simulations

Component	X_i (mol/mol)
Ca^{2+}	$1.33x10^{-4}$
$CO_{2,aq}$	0
HCO_3^-	$4.14x10^{-5}$
Na^+	$8.07x10^{-3}$
Cl^-	$9.08x10^{-3}$
Al^{3+}	$2.32x10^{-10}$
CO_3^{2-}	0
Mg^{2+}	$3.24x10^{-4}$
$SiO_{2,aq}$	$2.97x10^{-4}$
K^+	$9.50x10^{-5}$
Fe^{2+}	0

RESULTS

The aim of this study is to illustrate how CO_2 and water interacts with the solid mineral framework in the Utsira Sand. The main focus is to better understand the long-term potential of this reservoir for geological storage of injected CO_2. The simulated system is defined based on the Sleipner injection site where 1 Mt of CO_2 is annually injected (Chadwick et al., 2004). The final target of the Sleipner project is to inject for approximately 20 years, with a total injection of about 20 Mt CO_2 (Chadwick *et al*., 2004). We report here 20 years of injection and 980 years of post-injection reactive transport of CO_2.

Mineral reactions are on a short timescale, i.e. a few years, not assumed to significantly influence the amount of CO_2 stored in a reservoir, or change macroscopic flow variables such as porosity and permeability. Including mineral reactions may however significantly influence the water chemistry and especially the pH and the reactivity of water solutions with respect to solid mineral frameworks. This could for instance be of major importance with respect to corrosion of plugged abandoned wells. We report spatial and temporal evolution of pH that results from CO_2 injection in the Utsira Sand with and without pH buffering mineral reactions.

Data from well logs suggest that the Utsira Sand consists of several sand units separated by thin discontinuous clay horizons. The influence of these clay horizons on the retardation of immiscible CO_2 migration is suggested by seismic images shot after initiation of injection in 1996 (Chadwick et al., 2004). The clay horizons are also suggested to strongly influence the nature and spatial distribution of geological storage with time (e.g., Johnson *et al*., 2001; 2004). We present simulations that illustrate CO_2 injection into sand bodies that are separated by low-permeable discontinuous clay layers. The discontinuities are simulated by using sand lithologies with equivalent properties as the Utsira Sand used in the simulations. Finally, we show how the presence or absence of a regional flow through the system affects properties like CO_2 immiscible flow, CO_2 dissolution, pH distribution, and geological storage of CO_2.

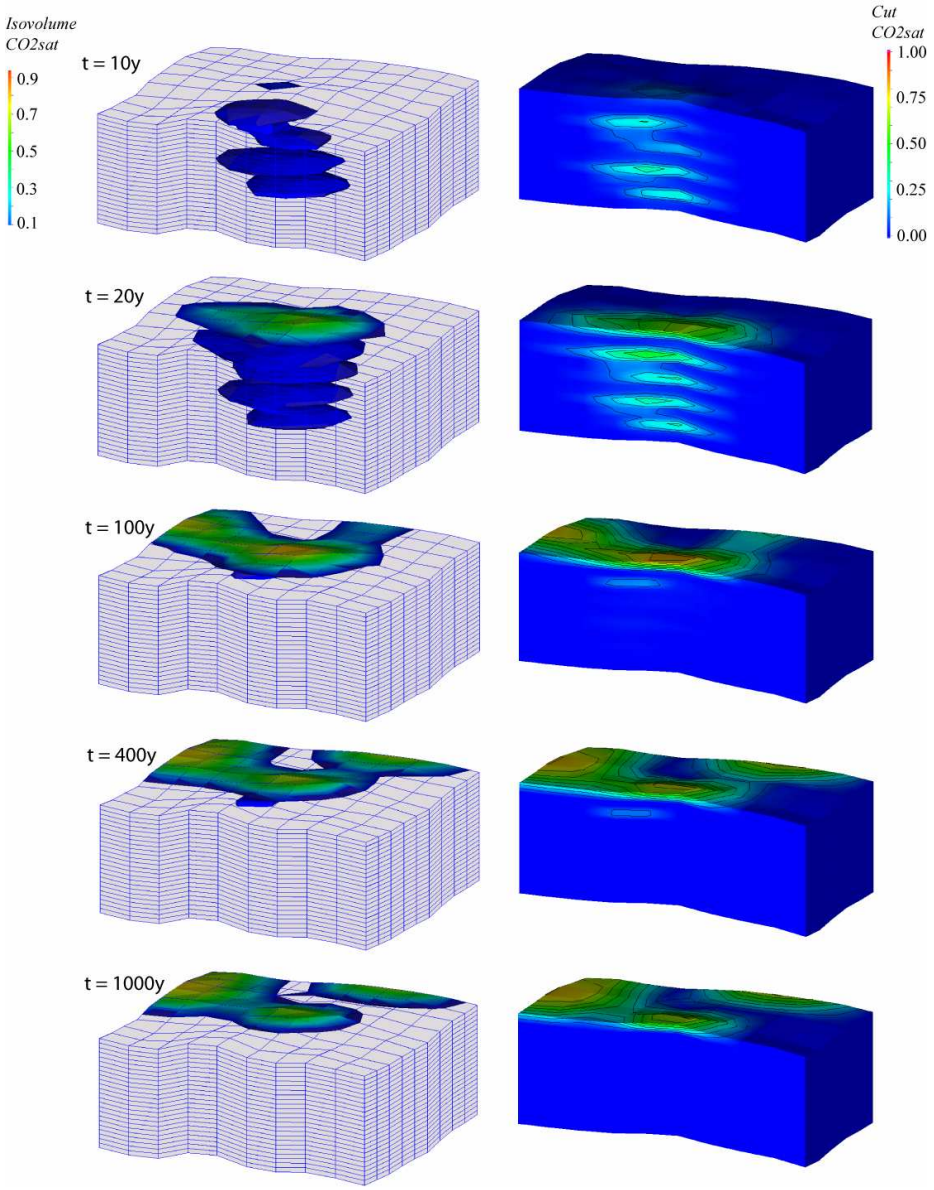

Fig. 4. CO_2 immiscible saturation in snapshots at 10, 20, 100, 400, and 1000 years. Isovolumes show the highest saturations between 0.1 and 0.9.

At each time *t*, results are reported as: Isovolumes that illustrate the highest reactivity, i.e. lowest pH, highest CO_2 saturations etc.; and cutplanes that show the reactivity in the central XZ plane where the CO_2 injector and discontinuities in clayey horizons occur.

CO_2 immiscible saturation

During and after CO_2 injection into a geological formation, some of the CO_2 dissolves into the aqueous phase, whereas the immiscible part may be mobilized due to buoyancy forces. The amount of CO_2 that is dissolved at a given time is determined by the temperature and pressure of the formation, the salinity of the aqueous solution, and the rate which the immiscible CO_2 is mobilized and get in contact with subsaturated water. Mineral reactions that consume CO_2 from the aqueous solution, as is the case for solid carbonate precipitation, consume immiscible CO_2 indirectly through the water phase. The immiscible CO_2 is trapped by low-permeable structures or alternatively spills out and migrate further towards the surface. Knowledge of immiscible CO_2 mobility is of major importance with respect to evaluate the risk of leakage to the surface.

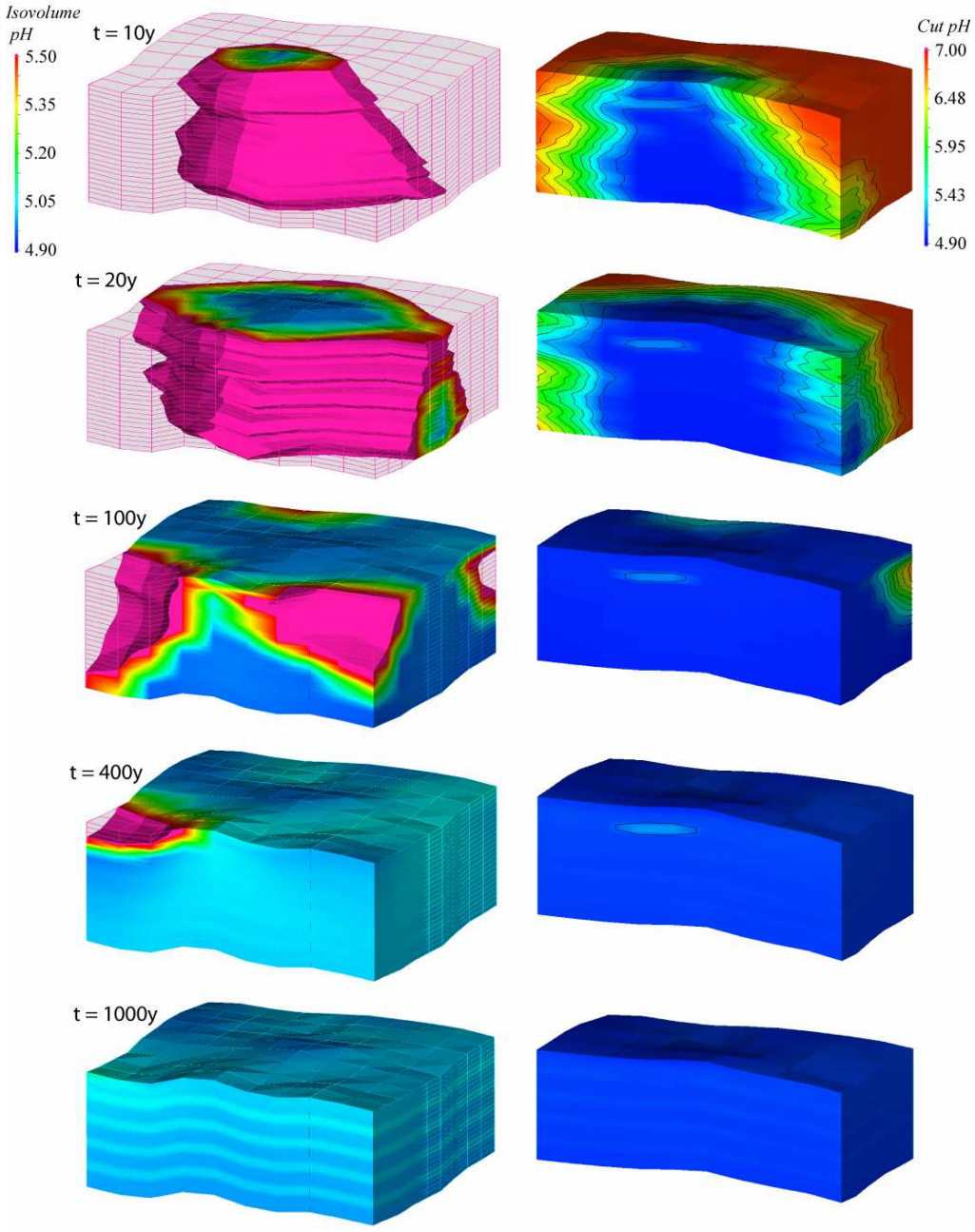

Fig. 5. pH illustrated in snapshots at 10, 20, 100, 400 and 1000 years. The isovolumes shows the spatial distribution of the areas with the highest aqueous CO_2 saturations and hence the lowest pH.

The Utsira Sand extends laterally for tens of kilometres and is at the Sleipner injection site covered with several hundred meters of low-permeable clays (Chadwick *et al.*, 2004). It is thus not likely that immiscible CO_2 will pose a leakage threat for this injection site. The mobility is however of major importance with respect to the spatial reactivity of the Utsira Sand.

Fig. 4 shows the temporal evolution of immiscible CO_2 in the Utsira Sand. Five snapshots are presented for the first 20 years during the CO_2 injection period and at 80, 380, and 980 years after injection ceased.

At 10 and 20 years during injection, immiscible CO_2 is spread as a continuous stream from the injector and up to the top of the formation. The injection rate is higher than the consumption rate into the aqueous phase and both the saturation level and spatial extension increases. The preferred path of the stream is through the low-permeable holes in the clayey layers, whereas a significant amount of CO_2 is retained below structural highs in the clay horizons.

After the injection is stopped at 20 years, CO_2 continues to migrate upwards and simultaneous dissolve in the aqueous solution. Less than 80 years after the injection stopped most CO_2 is trapped in topographic highs in the top of the formation. Some minor amount of immiscible CO_2 is still present trapped by the uppermost clay horizon. During the next 900 years until the end of the simulation at 1000 years, immiscible CO_2 changes little both with respect to spatial extension and distribution at the top of the formation. This suggests that the formation water that is in vicinity of the immiscible CO_2 is close to saturation already at 100 years. This is confirmed by the *pH* change with time presented in the next section.

Temporal and spatial evolution of *pH* in the Utsira simulation

One of the major effects CO_2 injection has on pore water chemistry is a significant drop in *pH* that follows formation and dissociation of carbonic acid. The *pH* drop is partly buffered by mineral reactions and especially carbonates that are present in the reservoir prior to injection. The resulting *pH* is instrumental in the reactivity of the reservoir minerals during CO_2 injection.

Fig. 5 illustrates the temporal and spatial evolution of *pH*. By comparing pH evolution with the CO_2 flow presented in the previous section we see that the two are clearly related. Areas around the immiscible flow where CO_2 dissolves to saturation show the largest decrease in pH. At 10 and 20 years during and at the end of CO_2 injection, a zone of low pH spreads around the injector and up to the top of the formation. The lowest pH values are in the central part where it drops rapidly from initial 7.0 to around 4.9. This value is at full CO_2 water saturation equilibrated with calcite that are present in both the sand and clayey layers. As the time proceeds, more and more of the system is affected by CO_2 dissolution, and the whole system approaches a pH of around 5.0. At 100 and 400 years the pH drop is seen to be strongly asymmetric in the system. This is caused by preferential CO_2 flow and dissolution to the highest topographies beneath clayey horizons and the top of the formation as seen in Fig. 4. Topographic lows on the other hand are less affected by the CO_2 injection. The upper left corner of the system shows such a topographic low. The pH in this region stays largely unaffected by the CO_2 injection for more than 400 years. At 1000 years at the end of the simulation the pH in this area also drops beneath 5.5 and approaches the values of the remaining sands. The evolution of acidity from 100 to 1000 years proceeds towards a uniform low value. Isovolumes shows that after the rapid initial drop in pH to approximately 4.9, slow mineral reactions change the pH to approximately 5.0. At 1000 years the pH of the clayey layers are uniformly at a slightly higher pH than the sands. The magnitude of mineral reactions presented in the next sections suggests that this is not caused by a higher reactivity in the clayey horizons, but can instead be explained by a smaller aqueous volume in the low-porosity clays which responds faster to mineral reactions.

Major mineral reactions

Geological storage of CO_2 is the conversion of injected mobile gaseous or supercritical CO_2 into solid carbonate minerals that may be stable and immobile for thousands of years. The geological storage is mainly driven by dissolution of primary minerals in the formation caused by increased acidity imposed by CO_2 injection (see previous section). The primary minerals that are important with respect to geological storage are minerals that contain components for possible carbonates i.e., mainly divalent cations like Fe^{2+}, Mg^{2+} and Ca^{2+}. These dissolved cations combine with dissolved carbonate to form stable mineral carbonates according to:

$$M^{2+} + 2HCO_3^- \rightarrow MCO_3 + H_2O + CO_{2,aq} \quad (12)$$

where one mole of a aqueous divalent cation M^{2+} precipitates one mole of solid M-carbonate immobilizing one mole of dissolved carbonate.

Major silicate reactions

Four phyllosilicates which are possible divalent cation sources, clinochlore-14A, daphnite-14A, annite, and phlogopite, are included as primary minerals in the present simulations (Table 3). We present the spatial and temporal evolution of the three former silicates that totally dominates as a source for divalent cations (Fig. 6). Phlogopite is not shown here because it is by total a minor source mineral compared to any of the three others. Since the phyllosilicates reactions are slow, we chose to illustrate only the late-stage images for these reactants.

Fig. 6 shows the relative change in volume fractions between initial values and values at time τ ($x_{t=\tau} - x_{t=0}$) for the three dominant phyllosilicate reactions. The figure suggests that the spatial reactivity is very similar for the three minerals. This is not surprising since they are all subsaturated at the acidic conditions induced by the CO_2 dissolution, and that the reaction kinetics of the three is very similar (see Table 3).

Common for the three minerals is that the highest reactivity is located where the aqueous solution has been saturated with CO_2 for the longest period. This means that the central part shows most dissolution whereas margins, especially at the topographic lows of the clayey layers are less reactive.

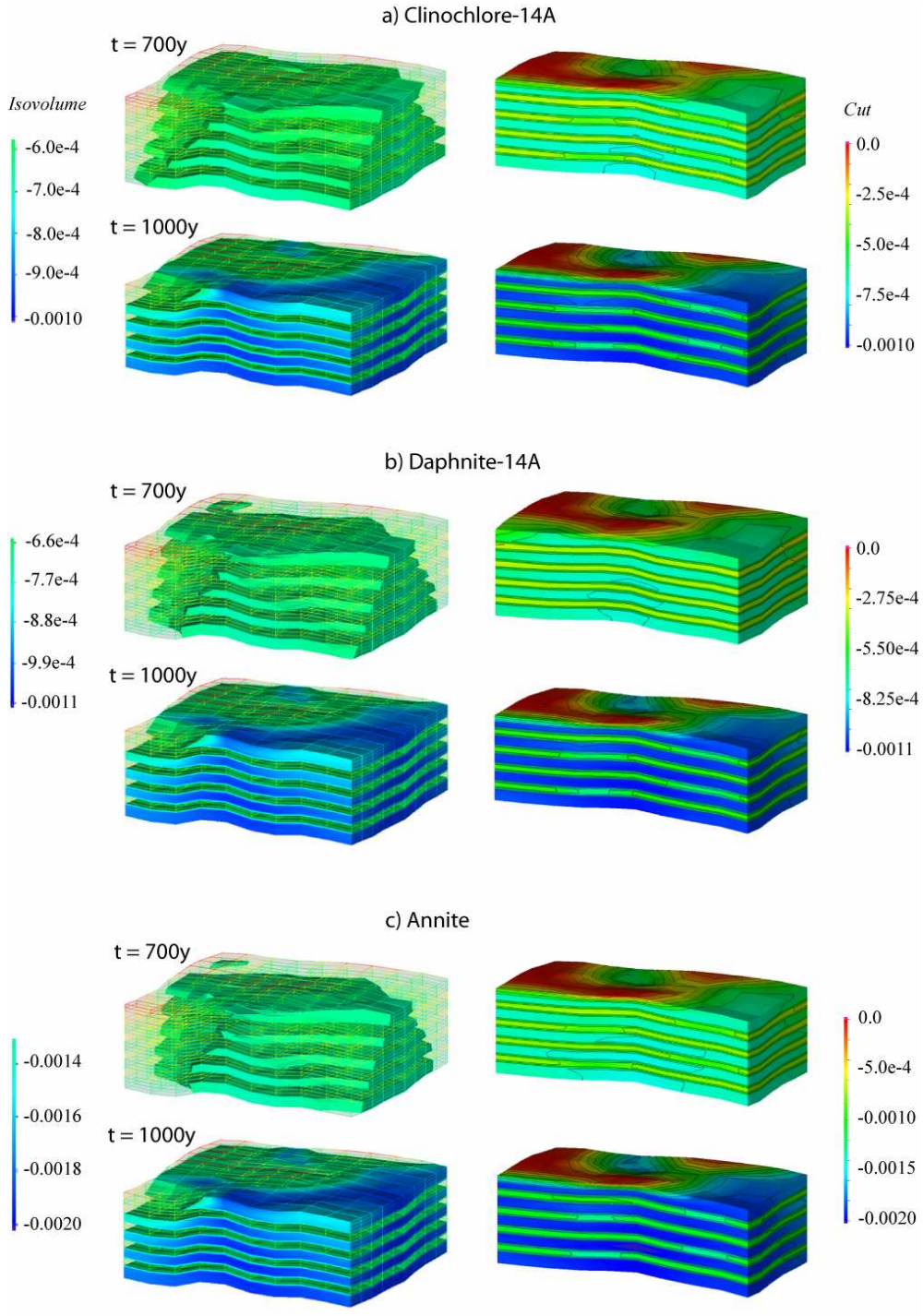

Fig. 6. Change in volume fraction of phyllosilicates from initial values to values at time *t*.. Snapshots at the latest stage of the simulation at 700 and 1000 years.

Other parts of the formation that are less reactive are locations that retain a high immiscible CO_2 saturation for long periods. This is especially the case for the topographic highs at the top surface that retains a high CO_2 saturation throughout the simulation. It is also a marked difference in the amount that dissolves in the clayey layers relative to the sandy units. The amount that dissolves of the former is approximately half that of the latter.

The maximum dissolution of clinochlore-14A, daphnite-14A, and annite is 0.10, 0.11 and 0.2 volume percent respectively.

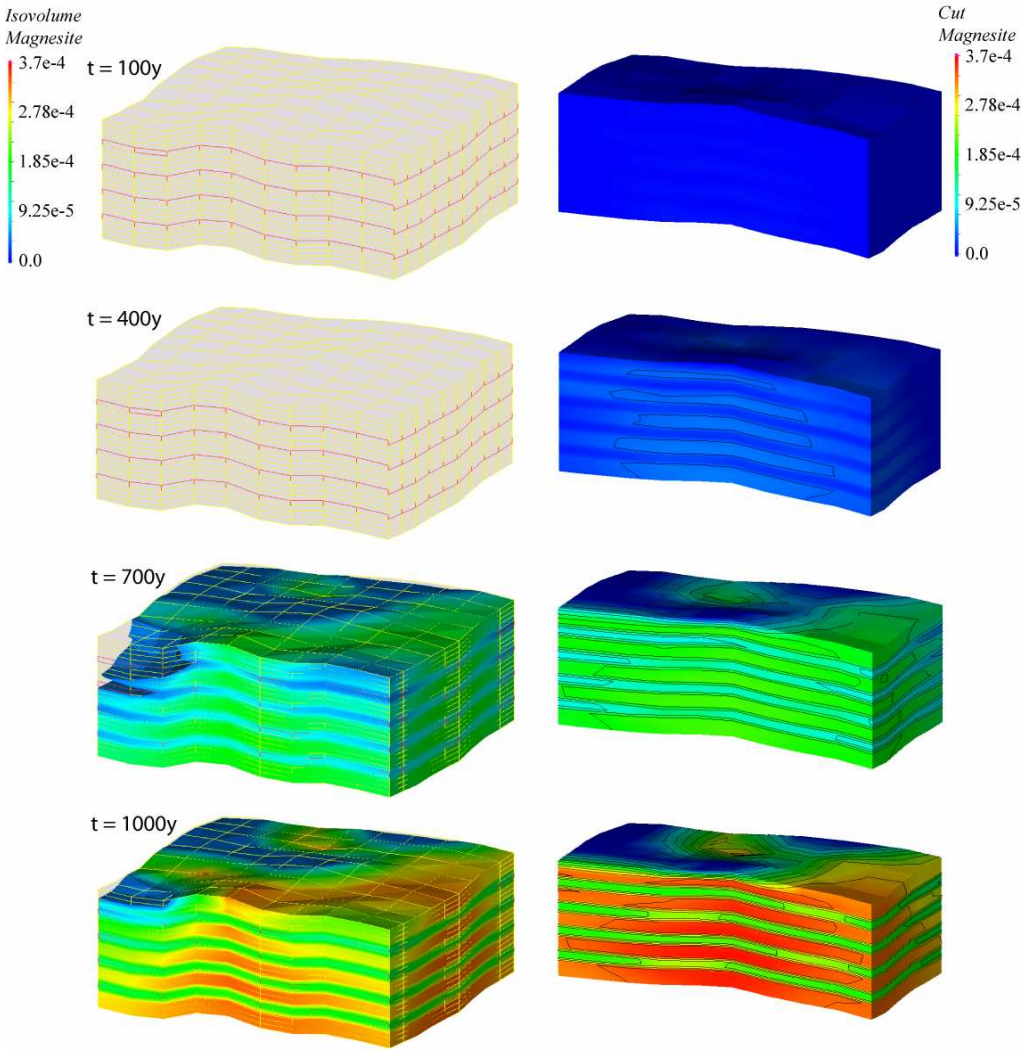

Fig. 7. Volume fraction of magnesite precipitated. Snapshots at 100, 400, 700 and 1000 years presented.

For each clinochlore-14A unit that dissolves, five units of Mg^{2+} are added to the aqueous solution. The dissolution reaction at acidic conditions can be written as:

$$\mathrm{Mg}_5Al_2Si_3O_{10}(OH)_8 + 16H^+ \rightarrow 5Mg^{2+} + 2Al^{3+} + 3SiO_{2,aq} + 12H_2O \quad . \qquad (13)$$

Daphnite-14A and annite provide five and three units of iron per unit mineral that dissolves respectively, and the dissolution reactions at acidic conditions can be expressed as:

$$Fe_5Al_2Si_3O_{10}(OH)_8 + 16H^+ \rightarrow 5Fe^{2+} + 2Al^{3+} + 3SiO_{2,aq} + 12H_2O \quad , \qquad (14)$$

and

$$\mathrm{K}Fe_3AlSi_3O_{10}(OH)_2 + 10H^+ \rightarrow K^+ + 3Fe^{2+} + Al^{3+} + 3SiO_{2,aq} + 6H_2O \quad . \qquad (15)$$

Major carbonate reactions

Dissolution reactions (13) to (15) give rise to precipitation of magnesite ($MgCO_3$) and siderite ($FeCO_3$) as the two dominating carbonates. The amount that precipitate out of each is mainly controlled by the individual kinetics of the dissolution reactions since they are several orders slower than the precipitation reactions of magnesite and siderite (see Table 3 for kinetic constants).

The reactivity of magnesite and siderite during 1000 years is illustrated in Fig. 7 and 8 respectively.

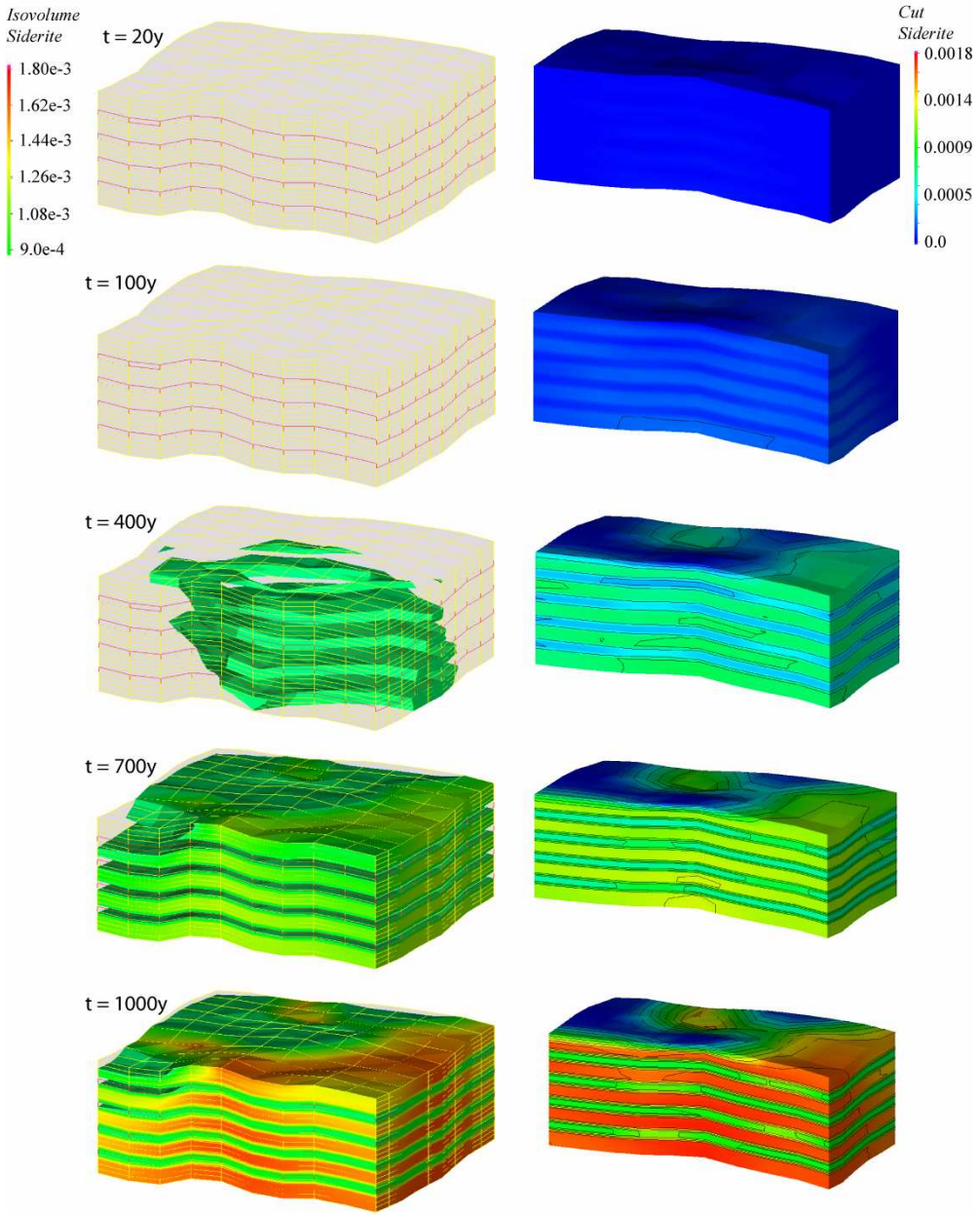

Fig.8. Volume fractions of siderite precipitated. Snapshots at 20, 100, 400, 700 and 1000 years.

The amount that precipitates and the spatial extent of the reactivity are highly connected to the spatial distribution of reactivity of the phyllosilicates. The highest reactivity is located in the central part where water solutions have been saturated with CO_2 for the longest period. The topography of the top of the formation and clayey horizons affects the trapping of immiscible CO_2, and locations with prevailing high CO_2 saturations, such as the topographic highs, show lower reactivity than topographic lows. Since the kinetics of the three dissolving phyllosilicates are similar, and daphnite-14A and annite in total contribute more Fe^{2+} to the solution than clinochlore-14A alone produces aqueous Mg^{2+}, more siderite is formed than magnesite. Snapshots at 20, 100, and 400 years shows that only minor amounts of carbonate precipitates at the first half of the simulation. This changes significantly to significantly higher precipitation rates during the second half of the simulation. At 1000 years the maximum amount of siderite and magnesite is 0.18 and 0.037 volume percent respectively.

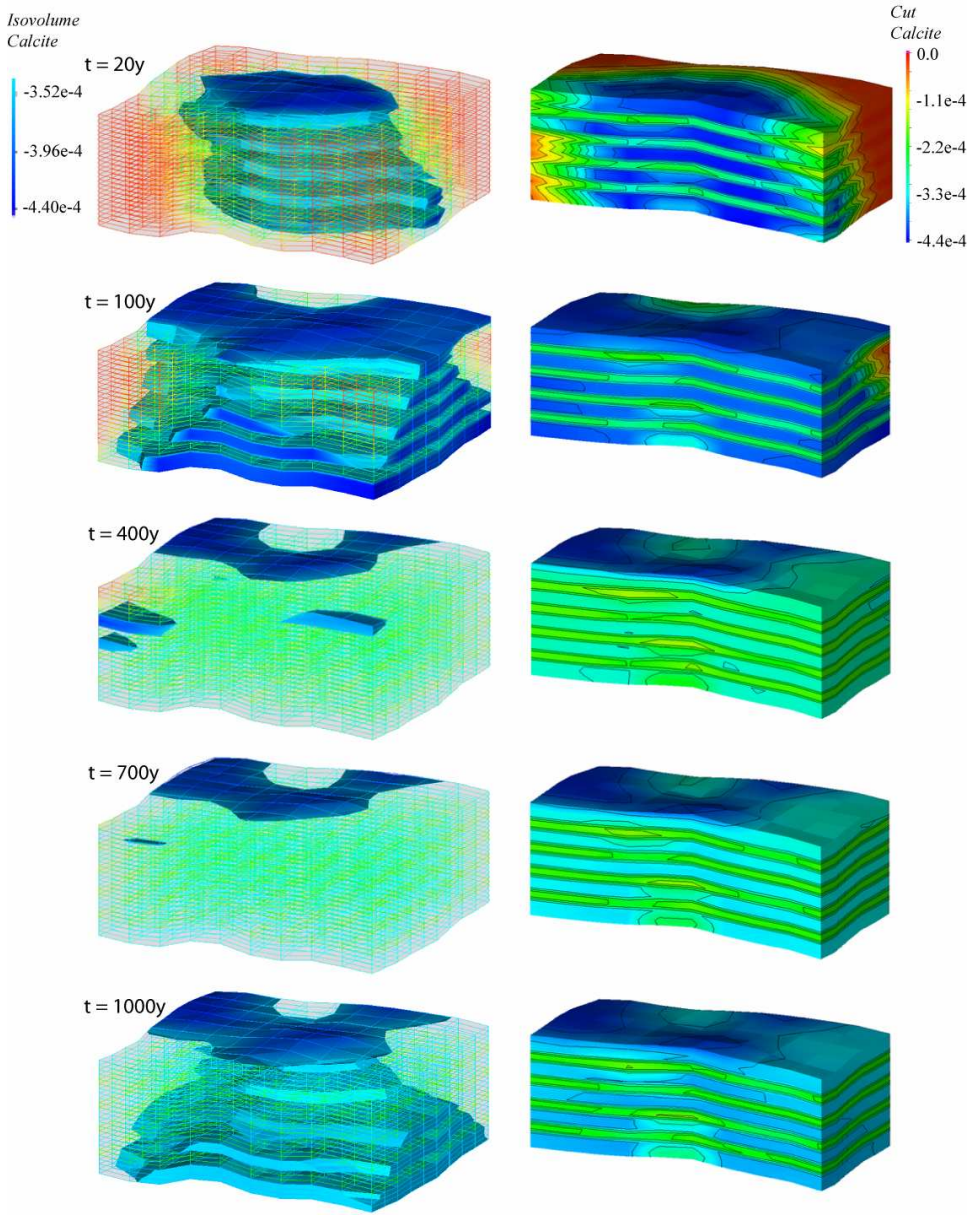

Fig. 9. Change in volume fraction calcite from initial value to values at time *t*. Snapshots presented at 20, 100, 400, 700 and 1000 years.

Expressions (13) to (15) suggest a 3/1 or 5/1 ratio between the amount of siderite and magnesite that precipitate and the amount of phyllosilicates that dissolve. This is however not the case. What is observed, especially in the first several hundred years, is that significantly less siderite is formed than expected based on the combined annite and daphnite-14A dissolution. This is explained by progressively higher concentrations of Fe^{2+} and Mg^{2+} in the aqueous solutions. This explains why the precipitation rate of the two carbonates is modest until the latest stage of the simulation. By extending the simulations to longer timespans we would expect a steady high precipitation rate and a significant increase in the geological storage.

Calcite is initially present as a primary mineral at close to saturation with the aqueous solution. As CO_2 is injected, calcite stability is shifted and it starts to dissolve. Since no calcium sources, such as labradorite, are present initially in the system, calcite is expected to show a net dissolution during the whole simulation time, i.e. amount present locally at time $t=\tau$ is always less or equal to the initial amount at $t=0$. Fig. 9 illustrates the spatial change in calcite volume fraction with time.

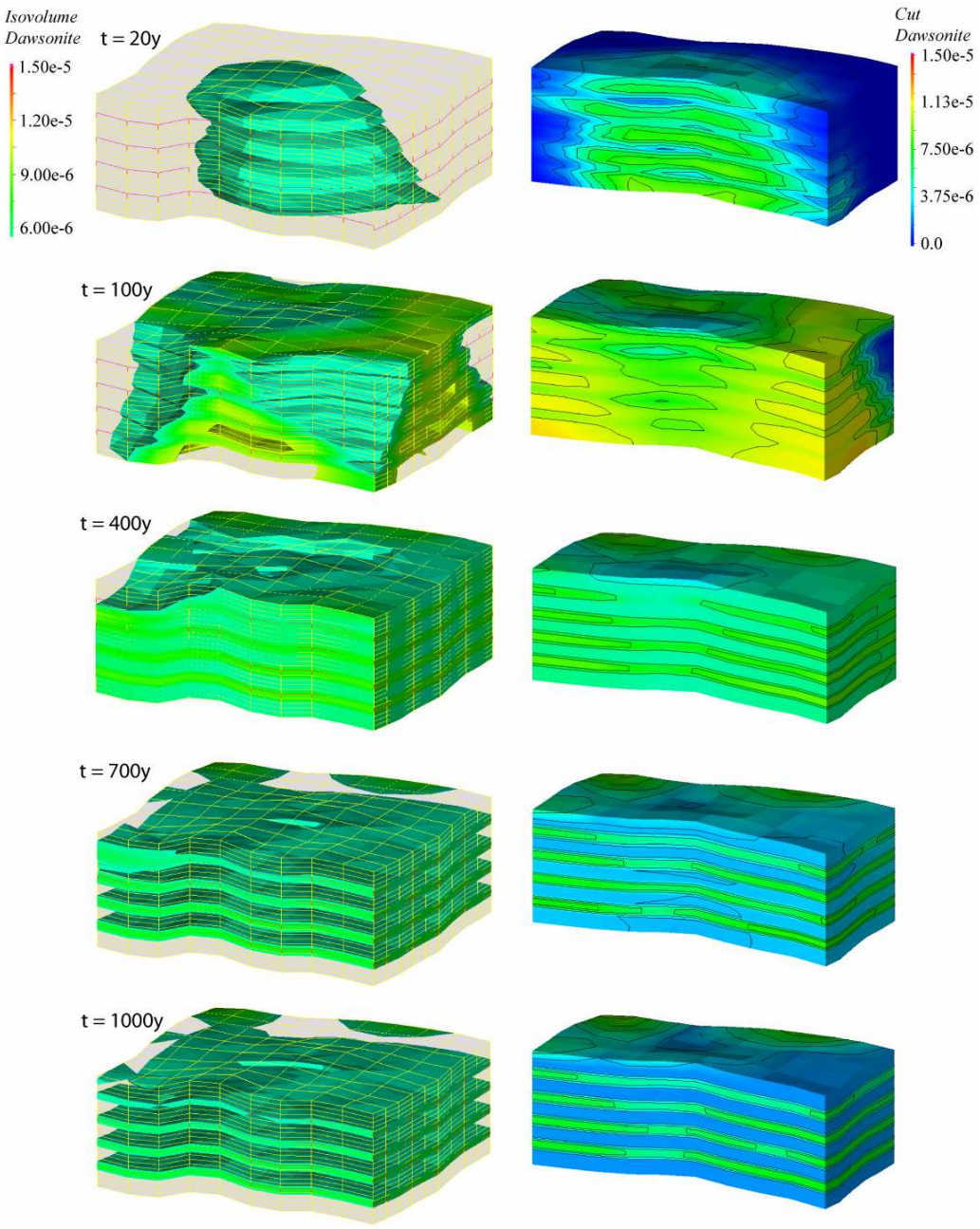

Fig. 10. Volume fraction dawsonite precipitated. Snapshots presented for 20, 100, 400, 700 and 1000 years.

Calcite starts, as expected, to dissolve in the central part of the system where aqueous CO_2 saturation is at its highest. As the CO_2 saturated part of the system increases, so does the extent of calcite dissolution. The amount of calcite that dissolves is however not just a simple function of the saturation level of CO_2. Fig. 9 suggests that calcite dissolves in a progressively larger part of the system and reach a maximum dissolution at some time before 1000 years. Reprecipitation is however observed, even though of minor magnitude, if we compare snapshots from 100, 400 and 700 years, whereas dissolution again occurs at the latest stage of the simulation. This dynamic behaviour is a result of competitions between the different carbonate reactions in addition to the dynamics of the aqueous CO_2 saturations. The dissolution at the late stage is for example caused by magnesite and siderite precipitation that is forced by the increasing Mg^{2+} and Fe^{2+} concentrations in the aqueous solution, which results in depletion of aqueous carbonate and enhanced calcite dissolution.

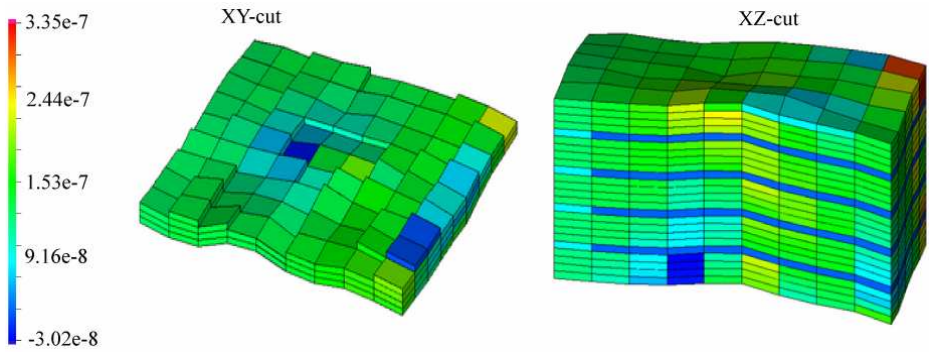

Fig. 11. Flowfield through the simulated volume in a lower XY surface beneath the lowermost clayey horizon and a profile through the central XZ cutplane.

Dawsonite reactivity

The thermodynamic stability of dawsonite suggests that it is stable and precipitate in any NaCl rich solution saturated with CO_2 at the Utsira physical conditions as long as aluminium is available for the reaction. The aluminium is generally available through the dissolution of aluminosilicates like the phyllosilicates presented in the previous section. Fig. 10 shows the spatial evolution of dawsonite volume fractions with time. The figure suggests a similar spatial distribution as the major silicate reactions. Initially it starts to form in the central part where the aqueous CO_2 saturation is high. It then precipitates in a wider and wider area proportionally with the widening of the CO_2 saturated area. The cutplane at 100 years shows the maximum extension of dawsonite precipitation. The volume fraction precipitated is less than 5% and 1% of the precipitated magnesite and siderite respectively. At 400 years the spatial extension increases, but the earlier formed dawsonite has started to dissolve. At 700 and 1000 years the dissolution continues and the final amount of dawsonite formed is low. This result is comparable with calculations of the lifetime of dawsonite that suggest that once the fugacity of CO_2 drops below a critical level, dawsonite is destabilized and starts to dissolve (Hellevang *et al*., 2005). In the present reactive transport simulation, most of the reservoir is below the bubble point value for CO_2, which destabilizes the early formed dawsonite.

Effects of a regional formation water flow on geological storage of CO_2

We have seen in previous sections that the buoyant flow of immiscible CO_2 migrates to topographic highs beneath low-permeable clayey layers and beneath the top seal. After some time most of the formation water is saturated with CO_2 and the immiscible phase reaches a steady state at topographic highs. We have also seen how the spatial distribution of CO_2 in the formation is instrumental in defining the pH, and the reactivity of mineral phases. In this section we present a simulation using the same system definition as in the previous simulation (see Fig. 3), but with a regional flow of formation water of approximately 1 m/y perpendicular to the YZ plane. Fig. 11 shows snapshots at 100 years of simulation of two sections, XZ and XY, which are parallel to the regional flow. The figure suggests that the regional flow leads to an average direction of the flow through the system, but that stagnant zones occur locally.

We illustrate the reactivity of the system by presenting the spatial evolution of the CO_2 immiscible phase and the pH evolution (Fig. 12). CO_2 immiscible saturations and the pH range (0.1 to 1.0 and 4.9 to 5.5 respectively) used for the isovolumes are the same here as for the previous simulation. During the first 20 years of injection the plume of immiscible CO_2 looks much the same as for the stagnant case. The same is the case for the pH evolution. Both pH and CO_2 saturations are however more asymmetric and shifted slightly more to the right-hand side of the system. After 100 years of simulation the effect of the flow is much more evident. The immiscible CO_2 and acidified formation waters now principally occupy the right-hand half of the system, whereas the left-hand half is largely unaffected by the injection. During the next 900 years most of the immiscible CO_2 is dissolved in the formation water and the pH approach a value of approximately 5 buffered by mineral reactions. Two features are worth noting from these simulations: (1) more CO_2 dissolved when having a regional flow through the system that 'refreshes' the formation waters in contact with the CO_2 phase; and (2) a regional flow of 1m/y has dramatic effects on where the immiscible CO_2 accumulates beneath the topographic highs.

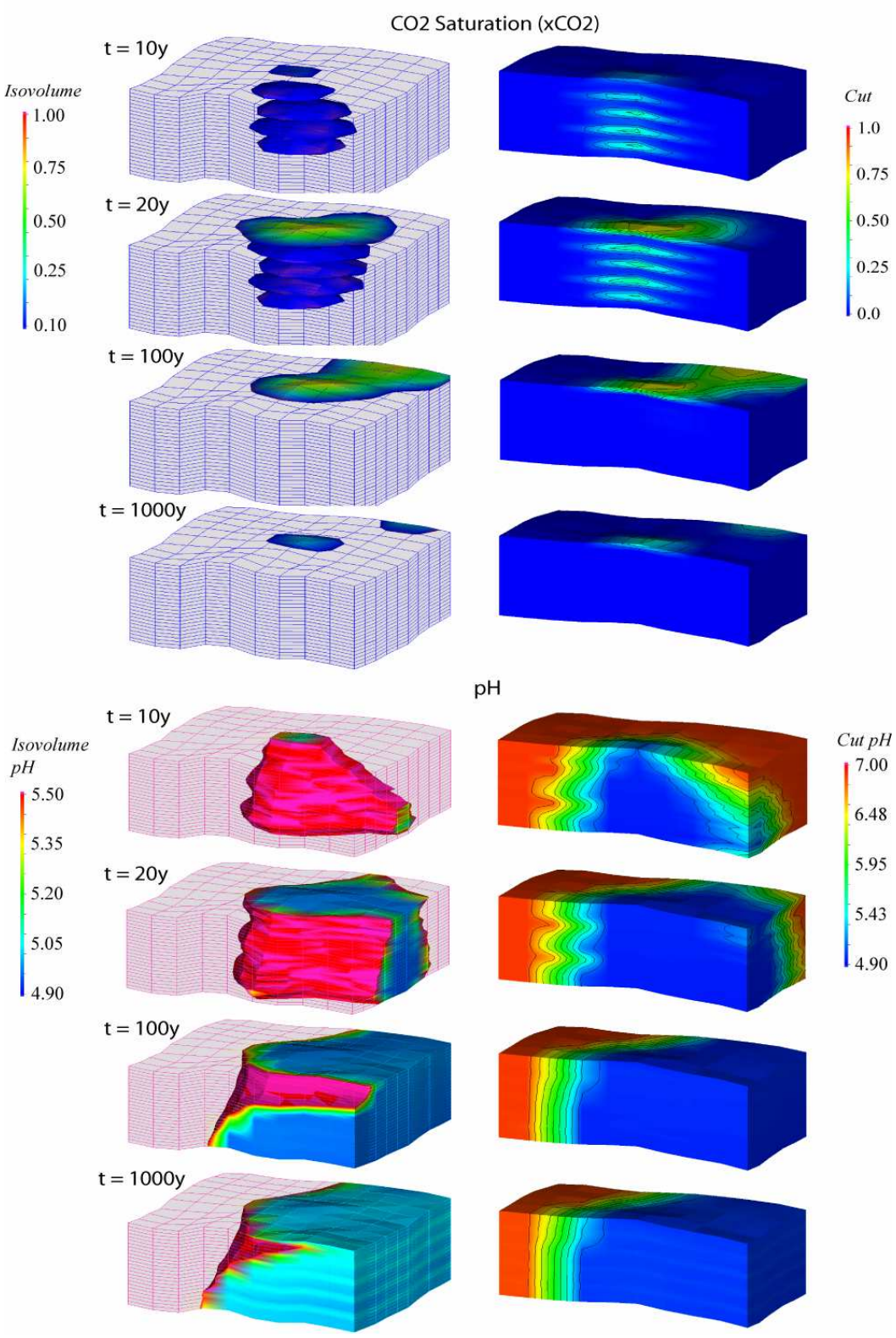

Fig. 12. Immiscible CO_2 saturation and pH shown for the second simulation where a regional flow of approximately 1m/y affects the system.

DISCUSSION

Comparisons of seismic profiles through the Sleipner injection site before and after CO_2 injection started provide us with information about the flow of CO_2 in the formation, and possibly of how the residual immiscible CO_2 is dispersed and dissolve in the formation with time. Seismic data is however limited by an upper resolution limit, and the data provides no direct information about interactions between injected CO_2, the formation water and the solid mineral framework. These interactions have to be measured or observed in laboratories or simulated by batch- or reactive transport numerical codes. The laboratory is excellent for measuring reactivity of isolated reactions or simple multi-component systems. It is however increasingly hard to gain information about reactions as systems get more complex and approach the complexity of natural systems. Multi-mineral-water-rock interactions at conditions that compare to natural systems are in addition commonly too slow to be measured during the time-scale of laboratory experiments. Numerical experiments on the other hand can provide information about complex long-term CO_2-water-rock interactions. The results of numerical simulations are however limited by the accuracy of input data like the thermodynamics and kinetics of mineral reactions. The following sections will briefly discuss results from the present numerical study of CO_2 injection, compare qualitatively the results with the results of other numerical simulations of similar systems, and do some comparisons with observed reactions in natural analogues. At the end we discuss briefly the possibility to simplify future reactive transport simulations by removing some of the complexities of the chemical interactions.

pH buffering by mineral reactions

Dissolution of CO_2 into the formation water leads to a decrease in pH with a maximum decrease at full CO_2 saturation. This increased acidity is buffered by dissolution of primary minerals that are present in the formation. The majority of these primary minerals are, in silisiclastic reservoirs like the Utsira formation, slow dissolving silicate minerals with a very limited buffering effect. It is however common that reservoir sands contain a small fraction of carbonate minerals such as calcite and aragonite. These are known to have reaction rates several orders higher than the silicates. Calcite is for instance commonly considered to react to equilibrium in a few hours or days if its equilibrium state is disturbed. The calcite dissolution reaction can be expressed by:

$$Calcite + CO_{2,aq} + H_2O \rightarrow Ca^{2+} + 2HCO_3^- , \quad (16)$$

where the important point with respect to understand the *pH* buffering effect of the reaction is the balanced addition of positive and negative charges to the solution by Ca^{2+} and HCO_3^- respectively. While Ca^{2+} is non-reactive in the solution, HCO_3^- is reduced by reactions with other species in the carbonate system (see Hellevang & Kvamme, 2006, for detailes). This leads to a net increase in positive charges in the solution. Using the criteria of electroneutrality we may express the concentration of H^+ in terms of all the other ion concentrations in the solution. Expression (17) shows pH defined by the sum of molar concentrations of all N dissolved ions excluding H^+:

$$pH = -\log_{10}\left\{-\gamma_{H^+}\sum_i^N m_i z_i \delta_i\right\},$$
$$\delta_i = 0 \text{ for } i = H^+$$
$$\text{and } \delta_i = 1 \text{ for other ions } i \quad (17)$$

where z is the charge, m is molar concentration and γ is the activity coefficient of H^+. From this expression we see that a net increase in positive charge induced by calcite dissolution results in a higher pH.

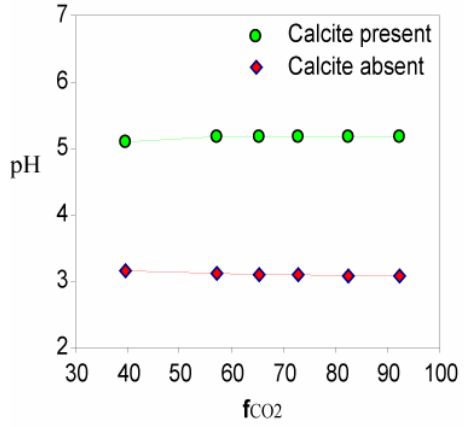

Fig. 13. pH calculated as a function of CO_2 fugacity at calcite equilibrium and without calcite present.

The magnitude of the buffering effect can be estimated by comparing pH in buffered solutions to numerical calculations excluding the mineral reactions. Fig. 13 illustrates how the presence or absence of calcite affects the pH at different CO_2 fugacities in a freshwater solution fully saturated with CO_2. The calculations are done with the ACCRETE geochemistry code using thermodynamic data calculated by the SUPCRT92 program with the dprons96.dat database. The figure shows that pH drops from initial 7 to approximately 3 if calcite is not equilibrated with the solution. The effect of

changing fugacity is minor. If the saturated solution on the other hand is equilibrated with calcite, pH only shows a moderate drop to approximately 5.1, which is comparable with the results observed for the Utsira Formation water in the present simulations.

CO_2 mobilization and consumption

Simulations presented here show that some immiscible CO_2 is still retained in topographic highs after 1000 years. Simulations also demonstrate that less CO_2 is retained in the system if a regional flow affects the system. In the case where a regional flow is present the immiscible CO_2 is dissolved locally by a continuous refreshing of the water phase. In the stagnant case on the other hand, only the slow conversion of CO_2 mainly to magnesite and siderite is responsible for the consumption of the CO_2 phase. This could lead to a free CO_2 phase for thousands of years in a stagnant system. This is however not very likely in natural systems, and the reason why this arises is that the boundaries of the system are closed for the exchange of immiscible CO_2 with the surroundings. In the real system immiscible CO_2 would migrate out of the system and get dispersed at the time when it accumulates at the boundaries. This situation arises after a few years in our simulations, as seen for the stagnant case in snapshots at 100, 400 and 1000 years (Fig. 4). In an open system that extends from the boundaries of the present simulated system we would expect faster dispersion of the aqueous CO_2 saturation, eventually to a reduction in the formation of solid carbonates locally, and more dispersed precipitation of carbonates in a larger volume.

Geological storage of CO_2

The outcome of numerical simulations of CO_2 storage is largely dependent on the choice of mineral assemblages, thermodynamic data, and by kinetic parameters of mineral reactions. Differences in primary mineralogy and physical conditions may lead to large differences both qualitatively and quantitatively with respect to solid carbonate precipitation (e.g., Xu *et al*., 2004; Hellevang & Kvamme, 2006). Hellevang & Kvamme (2006) shows that ACCRETE batch simulations compares qualitatively to batch- and reactive flow simulations by Xu *et al*. (2004), White *et al*. (2003), and Knauss *et al*. (2005), taking into account differences in primary mineralogies, and kinetic constants of mineral reactions. Most simulations suggest that the amount of secondary carbonates that precipitate out on a short timescale is limited. At timescales of thousands of years on the other hand, a significant part of injected CO_2 is immobilized by solid carbonate precipitation. The current study presents long-term reactive transport simulations that cover a large volume (~2.25km^3) centered around the CO_2 injection point. The mineralogy is based on the Utsira Sand and is adapted from Chadwick *et al*. (2004). The carbonates that dominate as storage hosts in the present numerical simulations are comparable with what is observed in Hellevang & Kvamme (2006). The major carbonates that precipitate are siderite and magnesite, resulting from dissolution of phyllosilicates that release Mg^{2+} and Fe^{2+} to the formation water. Dawsonite is a minor phase. The magnitude of the reactions are however low compared to the ACCRETE batch simulations because of larger timesteps in the ACCRETE mineral solver in this study compared to previous batch simulations. This strongly influences the activities of ions like Al^{3+} that are instrumental in the saturation states of the aluminosilicates. This can be seen from the ion activity product q of the aluminosilicate reactions:

$$q = \alpha \cdot \boldsymbol{a}_{Al^{3+}}^{\eta}, \tag{18}$$

where α is a coefficient containing the contribution from other ionic components to the ion activity product, and η is the stoichiometric number of Al^{3+} in the reactions. The saturation state of a mineral can be expressed by the solubility index as:

$$SI = \log\left(\frac{q}{K_{eq}}\right), \tag{19}$$

where K_{eq} is the equilibrium constant for the reaction. SI < 0 means subsaturation and mineral dissolution, whereas SI > 0 means supersaturation and precipitation. If the aluminosilicate reactions at a given time t results in a net consumption of Al^{3+}, its concentration decreases according to expression (11). This possibly results in a shift in reaction direction at time $t+1$ and a shift to net production of Al^{3+}. If, during a net consumption of Al^{3+}, the result of expression (11) for Al^{3+} is small relative to the absolute value of Al^{3+}, the mineral reactions proceed in a smooth fashion without jumping back and forth. If on the other hand expression (11) produces values that are close to the absolute value of Al^{3+} during a net consumption, its concentration will fluctuate and the aluminosilicate reactions will jump back and forth. This results in a conservative estimate of the mineral reactions that may give an order less overall mineral reactivity than optimal runs. Since natural reaction rates commonly are regarded as orders of magnitude slower than laboratory rates (e.g., Schnoor, 1990; Velbel, 1993; Blum, 2004; White, 2005) as used in the kinetic database, the error induced by the timestep size is regarded as acceptable. The major benefit of using the larger timesteps is substantial faster simulation time with possibilities of reactive transport simulations of large systems.

Can we simplify the complex chemical interactions in future numerical studies of CO_2 storage?

Chemical calculations in ACCRETE are divided into two solvers that are mutual dependent: (1) a solver that calculates the speciation of aqueous components; and (2) a mineral solver. The chemical speciation requires only a few iterations and is solved without much computational effort, whereas the mineral reactions are strongly non-linear and significantly harder to solve.

As suggested by this study as well as other numerical studies on CO_2 storage (e.g., Xu *et al*., 2004; Hellevang & Kvamme, 2006) the magnitude of many of the mineral reactions are, even after hundreds of years, minor. Inducing a regional flow that disperses the aqueous CO_2 saturation could in addition reverse some of the carbonate reactions. It is therefore natural to ask if the mineral reactions are insignificant and can be removed from the simulations. The answer to this question is of course dependent on the purpose of the simulations. For example, to obtain information regarding the short-term leakage potential of an injection site, mineral reactions would clearly be insignificant. If the purpose of a simulation is to see the evolution of injected CO_2 for thousands of years in systems that extend for tens or hundreds of km^3, mineral reactions may be significant, but not included because of the heavy computational processing required. It is however one mineral reaction that is significant both on short and long timescales, and should be considered if likely to be present in a system. Calcite reacts to equilibrium in hours or days and is instrumental in calculating the pH (Fig. 13) and thus the reactivity of the formation water. Since the calcite reaction is fast it can be considered as an instant equilibrium reaction and the extent λ of the reaction given in expression (16) to reach equilibrium can be calculated by solving:

$$\lambda^3 + \left(m_{Ca} + m_{HCO_3}\right)\lambda^2 + \left(\frac{4\boldsymbol{a}_{Ca}\boldsymbol{a}_{HCO_3}\gamma_{HCO_3} + \gamma_{Ca}\boldsymbol{a}_{HCO_3}^2 + K_{Calc}}{4\gamma_{Ca}\gamma_{HCO_3}^2}\right)\lambda + \frac{\boldsymbol{a}_{Ca}\boldsymbol{a}_{HCO_3}^2 - m_{CO_{2,aq}}K_{Calc}}{4\gamma_{Ca}\gamma_{HCO_3}^2} = 0, \qquad (20)$$

where γ, m, and $\boldsymbol{a}$ denote molar activity coefficient, molar concentration and activity respectively, and K_{Calc} is the equilibrium constant for reaction (16). Equilibrium is usually found from one single real root. Equation (20) has to be combined with the speciation calculations to assure that charge- and mass balance demands, as well as equilibrium among the carbon species are satisfied. If calcite is likely to be present in a system, adding the calcite reaction will not affect the simulation runtime to any significant extent, and it gives the simulations a good estimate of the reactivity of the system.

CONCLUSIONS

We have simulated 2.25km^3 of the Utsira Sand centred around the CO_2 injector at Sleipner. As CO_2 is injected immiscible CO_2 rises buoyantly and accumulates beneath low-permeable intra-formation clayey horizons and beneath the top of the formation in topographic highs. CO_2 dissolves in the formation water and pH decreases to around 5.0 in equilibrium with calcite. The fast calcite reaction is considered as instrumental in buffering the pH drop during CO_2 storage. It should therefore always be included as an equilibrium reaction if it is likely to be present in a system, even if the slower mineral reactions are considered insignificant. The acidic environment induces dissolution of primary minerals such as clinochlore-14A, daphnite-14A, and annite, which results in precipitation dominated by magnesite and siderite. Dawsonite precipitates only as a minor phase and dissolves at later stages of the simulations. Because of large timesteps in the mineral solver of ACCRETE, the reactivity of minerals in the present study is conservative estimates. The error induced is regarded as acceptable since laboratory rates as used in the ACCRETE code is known to overestimate reaction kinetics compared to natural systems. To see how a regional flow affects the spatial and temporal evolution of the injected CO_2, a flow of approximately 1 m/y was introduced to the system in a second simulation. The flow is seen to affect the spatial distribution of immiscible CO_2 strongly, and more CO_2 is consumed into the aqueous phase compared to the first simulation.

ACKNOWLEDGEMENTS

We are grateful to Jan Nordbotten for helpful discussions and valuable help during the development of an interface linking the ATHENA and ACCRETE numerical codes. Comments on the manuscript by Bjarte Hellevang were highly appreciated. We thank Tore Torp at Statoil Research Centre for letting us use Top-Utsira seismic data. This project was made possible through financial support by the Norwegian Research Council and Norsk Hydro through Grant 151400/210.

REFERENCES

BACHU, S., GUNTER, W.D. & PERKINS, E.H. (1994) Aguifer disposal of CO_2: hydrodynamic and mineral trapping. *Energy Convers. Manage.,* **35**, 269-279.

BAINES, S.J. & WORDEN, R.H., (2004) Geological storage of carbon dioxide. In: Baines, S.J., and Worden, R.H. (eds), Geological Storage of Carbon Dioxide. *Geological Society, London, Special Publications,* **233**, 1-6.

BLUM, A.E. (2004). Determining Dissolution, Precipitation and Nucleation Rate Laws in Natural Systems. Abstract, Workshop on Conceptual Model Development for Subsurface Reactive Transport Modeling of Inorganic Contaminants, Radionuclides, and Nutrients. Albuquerque, New Mexico, April 20-22, 2004.

BOUCHARD, R., & DELAYTERMOZ, A. (2004) Integrated path towards geological storage. *Energy*, **29**, 1339-1346.

CARROLL, S. A. & KNAUSS, K. G. (2005) Dependence of labradorite dissolution kinetics on $CO_{2(aq)}$, Al_{aq}, and temperature. *Chem. Geol.,* **217**, 213–225.

CHADWICK, R.A., ZWEIGEL, P., GREGERSEN, U., KIRBY, G.A., HOLLOWAY, S. & JOHANNESSEN, P.N. (2004) Geological reservoir characterization of a CO_2 storage site: The Utsira Sand, Sleipner, northern North Sea. *Energy,* **29**, 1371-1381.

CZERNICHOWSKI-LAURIOL, I., ROCHELLE, C. A., BROSSE, E., SPRINGER, N., BATEMAN, K., KERVEVAN, C., PEARCE, J.M., & SANJUAN, B. (2002) Reactivity of injected CO_2 with the Utsira Sand reservoir at Sleipner**.** *Abstract, GHGT6*, Kyoto, Japan, 1.-4.Okt.

ELEWAUT, E.F.M. (1997) Secondary Oil Migration Project, An Integrated Geochemical and Quantitative Modelling Approach for Understanding and Predicting Secondary Oil Migration. Tech. rep., Netherlands Institute of Applied Geoscience - TNO, National Geological Survey, Contract No. JOU2 CT93-0368.

FLADMARK, G.E. (1997) Secondary Oil Migration. Mathematical and Numerical Modelling in SOM Simulator. Tech. rep., Norsk Hydro ASA, E & P Research Centre, Bergen, Norway.

GANOR, J., MOGOLLON, J. L. & LASAGA, A. C. (2005) Kinetics of gibbsite dissolution under low ionic strenth conditions. *Geochim. Cosmochim. Acta* **63** (11-12), 1635–1651.

GARRIDO, I., ØYE, G.Å.,CHAIB, M., FLADMARK G.E. & ESPEDAL, M.S. (2004) Implicit treatment of compositional flow, *Comput. Geosci.,* **8**, 1-19.

GREGERSEN, U., MICHELSEN, O. & SØRENSEN, J.C. (1997) Stratigraphy and facies distribution of the Utsira Formation and the Pliocene sequences in the northern North Sea. *Mar. Petrol. Geol.,* **14**, 893-914

GREGERSEN, U., JOHANNESSEN, P.N., CHADWICK, R.A., HOLLOWAY, S. & KIRBY, G.A. (2000) Regional study of the Neogene deposits in the southern Viking Graben area - a site for potential CO_2 storage. 62nd EAGE meeting, Glasgow.

GUNTER, W.D., BACHU, S., LAW, D.H.S., MARWAHA, V., DRYSDALE, D.L., MACDONALD, D.E. & MCCANN, T.J. (1996) Technical and economic feasibility of CO2 disposal in aquifers within the Alberta Sedimentary Basin, Canada. *Energy Convers. Manage.*, **37**, 1135-1142.

HELLEVANG, H., AAGAARD, P., OELKERS, E.H. & KVAMME, B. (2005) Can dawsonite permanently trap CO_2? *Environ. Sci. Tech.,* **39**, 8281-8287.

HELLEVANG, H. & KVAMME, B. (2006) CO_2-water-rock interactions - ACCRETE simulations of geological storage of CO_2. *Submitted to Appl. Geoch.*

JOHNSON, J.W., OELKERS, E.H. & HELGESON, H.C. (1992) SUPCRT92: a software package for calculating the standard molal thermodynamic properties of minerals, gases, aqueous species, and reactions from 1 to 5000 bar and 0 to 1000°C. *Comput. Geosci.,* **18**, 899–947.

JOHNSON, J.W., NITAO, J.J., STEEFEL, C.I. & KNAUSS, K.G. (2001) Reactive transport modeling of geologic CO_2 sequestration in saline aquifers: The influence of intra-aquifer shales and the relative effectiveness of structural solubility, and mineral trapping during prograde and retrograde sequestration. *Proceeding*, First National Conference on Carbon Sequestration, Washington**.**

JOHNSON, J.W., NITAO, J.J., AND KNAUSS, K.G. (2004) Reactive transport modeling of CO2 storage in saline aquifers to elucidate fundamental processes, trapping mechanisms and sequestration partitioning. In: Baines, S.J., and Worden, R.H. (eds), Geological Storage of Carbon Dioxide. *Geological Society, London, Special Publications,* **233**, 107-128.

KNAUSS, K. G., JOHNSON, J. W. & STEEFEL, C. I. (2005) Evaluation of the impact of CO_2, co-contaminant gas, aqueous fluid and reservoir rock interactions on the geologic sequestration of CO_2. *Chem. Geol.* **217**, 339–350.

KORBØL, R. & KADDOUR, A. (1995) Sleipner vest CO_2 disposal – Injection of removed CO_2 into the Utsira Formation. *Energ. Convers. Manage.,* **36**, 509-512.

LASAGA, A.C. (1998) Kinetic theory in the earth science. Princeton University Press.

LOHUIS, J.A.O. (1993) Carbon dioxide disposa land sustainable development in the Netherlands. *Energy Convers. Manage.,* **34**, 815-821.

MALDAL, T. & TAPPEL, I.M. (2004) CO_2 underground storage for Snøhvit gas field development. *Energy,* **29**, 1403–1411.

QIN, G., WANG, H., EWING, R.E. & ESPEDAL, M.S. (2000) Numerical simulation of compositional fluid flow in porous media. In: Numerical treatment of multiphase flows in porous media, (Eds. Z.Chen, R.E.Ewing, and

Z.-C.Shi). Springer-Verlag, Berlin, 552, pp. 232-243.

REME, H. & ØYE, G.Å. (1999) Use of local grid refinement and a galerkin technique to study secondary migration in fractured and faulted regions. *Comp. Visual. Sci.,* **2**, 153-162.

REME, H., ØYE, G.Å., ESPEDAL, M.S. & FLADMARK, G.E. (2000) Parallelization of a compositional reservoir simulator, in Numerical treatment of multiphase flows in porous media, Beijing (Z.-C.S.Z. Chen, R. E. Ewing, ed.), no. 552 in Lecture Notes in Physics, pp. 244-267, Berlin: Springer Verlag.

REME, H., ESPEDAL, M. & FLADMARK, G.E. (2002) A preconditioning technique as an upscaling procedure, in Resource recovery, confinement, and remediation of environmental hazards (Minneapolis, MN, 2000), vol. 131 of The IMA Volumes in Mathematics and its Applications, pp. 283-297, New York: Springer Verlag.

RIDDIFORD, F., WRIGHT, I., BISHOP, C., ESPIE, T. & TOURQUI, A. (2004) Monitoring geological storage the In Salah gas CO_2 storage project. GHGT7, Vancouver, Canada, 5.-9.Sept.

SAYLOR, B., MATISOFF, G. & MORRISON, P. (2001) Geologic and geochemical evaluation of the potential for CO_2 disposal in deep saline aquifers beneath Ohio. *Proceeding*, First National Conference on Carbon Sequestration, Washington**.**

SCHNOOR, J.L. (1990) Kinetics of chemical weathering: A comparison of laboratory and field weathering rates. In Stumm, W. (Ed.): *Aquatic Chemical Kinetics: Reaction Rates of Processes in Natural Waters.* John Wiley & Sons, New York.

TORP, T.A. & GALE, J. (2004) Demonstrating Storage of CO_2 in Geological Reservoirs: The Sleipner and Sacs Projects. *Energy*, **29**, 1361-1369.

TRUESDELL, A.H. & JONES, B.F. (1974) WATEQ, a computer program for calculating chemical equilibria of natural waters. *J. Res.,* U.S. Geological Survey, **2**, 233–274.

VELBEL, M.A. (1993) Constancy of silicate-mineral weathering-rate ratios between natural and experimental weathering: implications for hydrologic control of differences in absolute rates. *Chem. Geol.,* **105**, 89-99.

WHITE, S. P., ALLIS, R. G., MOORE, J., CHIDSEY, T., MORGAN, C., GWYNN, W. & ADAMS, M. (2003) Injection of CO_2 into an unconfined aquifer located beneath the Colorado, Central Utah, USA. In: Proc. 2nd. Nat. Conf. Carb. Seq., Alexandria, VA, May 5-8.

WHITE, A. (2005) Controls on on rates of silicate mineral weathering. GSA Annual Meeting, Salt Lake City, October 16-19, 2005.

XU, T., APPS, J. A. & PRUESS, K. (2004) Numerical simulation of CO_2 disposal by mineral trapping in deep aquifers. *Appl. Geochem.* **19**, 917–936.

ZWEIGEL, P., HAMBORG, M., ARTS, R., LOTHE, A., SYLTA, Ø. & TØMMERÅS, A. (2001) Results and experiences from the first industrial scale underground CO_2 sequestration case (Slepiner Field, North Sea). AAPG, Annual Meeting, June 2001, Denver, abstract volume (CD) 6p.

ØYE, G.Å. & REME, H. (1999) Parallelization of a compositional simulator with a galerkin coarse/fine method, in EuroPar'99 Parallel Processing (P. Amestoy, P. Berger, M. Daydé, I. Du, V. Frayssé, L. Giraud, and D. Ruiz, eds.), Lecture Notes in Computer Science, No. 1685, pp. 586-594, Springer-Verlag, Berlin.